Constraining the magnetic field in the parsec-scale jets of the brightest *Fermi* blazars with multifrequency VLBI observations

K.V. Sokolovsky*, Y.Y. Kovalev
MPIfR, Bonn, Germany and ASC Lebedev, Moscow, Russia
A.P. Lobanov, T. Savolainen
MPIfR, Bonn, Germany
A.B. Pushkarev
MPIfR, Bonn, Germany; Pulkovo Obs., St Petersburg, Russia; CrAO, Crimea, Ukraine
M. Kadler
Dr. Remeis-Sternwarte & ECAP, Bamberg, Germany; CRESST/NASA GSFC and USRA, MD, USA

The spatially resolved broad-band spectroscopy with Very Long Baseline Interferometry (VLBI) is one of the few methods that can probe the physical conditions inside blazar jets. We report on measurements of the magnetic field strength in parsec-scale radio structures of selected bright *Fermi* blazars, based on fitting the synchrotron spectrum to VLBA images made at seven frequencies in a 4.6–43.2 GHz range. Upper limits of $B_\perp \leq 10^{-2}$–10^{2} G (observer's frame) could be placed on the magnetic field strength in 13 sources. Hard radio spectra ($-0.5 \leq \alpha \leq +0.1$, $S_\nu \sim \nu^\alpha$) observed above the synchrotron peak may either be an indication of a hard energy spectrum of the emitting electron population or result from a significant inhomogeneity of the emitting region.

1. Introduction

Blazars are active galactic nuclei characterized by highly variable non-thermal continuum emission across the electromagnetic spectrum. The Large Area Telescope (LAT, [1]) on board the *Fermi* γ-ray observatory, launched on 2008 June 11, provides a wealth of new information about high-energy radiation of blazars. It is believed that this high-energy emission is intimately connected with the emission at lower energies (radio – optical) through the process of inverse Compton scattering. Very Long Baseline Interferometry (VLBI), with its spectacular angular resolution, provides the most detailed view of inner regions in blazars [2]. In most cases, VLBI observations reveal one-sided relativistically beamed parsec-scale jets originating in a bright, compact region called the "core".

The spatially resolved broad-band spectroscopy is one of the few methods that can probe the physical conditions inside blazar jets. Despite the great potential of this method, its applications are still relatively rare (see [3] and references therein), owing to difficulties in implementing it and interpreting results obtained [4]. In addition, multifrequency VLBI observations require large amounts of observing time and most VLBI arrays lack technical capability to perform simultaneous multifrequency observations.

We utilize the Very Long Baseline Array (VLBA, [5]) which has a unique capability to conduct observations quasi-simultaneously at many frequencies, needed to constrain physical conditions in the regions where blazar radio emission originates. We reconstruct radio spectra of parsec-scale features in jets of selected γ-ray-bright blazars and compare them with the simple homogeneous synchrotron source model, which allows us to derive information about the magnetic field strength and particle energy distribution. During the first year of the *Fermi* scientific operations, we used the VLBA to observe 20 blazars, that were identified prior to the launch of *Fermi* as expected bright γ-ray emitters. In this paper, we present results for 17 of them. The data analysis for three remaining sources is still ongoing.

2. Observations and data reduction

The observations were conducted simultaneously at seven frequencies in a 4.6–43.2 GHz range. After the initial calibration in the *AIPS* package [6], the sources were self-calibrated and imaged independently at each frequency using the *Difmap* software [7]. Whenever feasible, the frequency-dependent core position (the "core shift" effect, see for a detailed discussion [8, 9]) was taken into account. Image alignment is a major problem for spectral VLBI analysis because the self-calibration technique used to obtain high-quality images causes loss of information about the absolute position of a source. Positions of optically thin jet features or the core itself (if the "core shift" effect is negligible for a given source) are then used to align VLBI images obtained at different frequencies.

In order to reconstruct the spectrum in a given pixel of an image ("pixel-based approach"), the sum of CLEAN components around this pixel was used. The CLEAN components were summed in-

*Send offprint requests to K.V. Sokolovsky
e-mail: ksokolov@mpifr-bonn.mpg.de

side a radius $R = \Theta(\text{lowest frequency})/3$, where Θ(lowest frequency) is the half-power beam width at the lowest observing frequency (4.6 GHz). This approach has a major advantage over the direct use of flux densities from reconstructed images because it avoids artifacts introduced by convolution with a Gaussian beam while preserving the angular resolution achieved.

3. Results

The radio spectra in the parsec-scale core regions (marked as shaded areas on Fig. 1) of the observed blazars have diverse properties. Most of them are nearly flat, with signs of curvature at lower frequencies, which we interpret as synchrotron self-absorption. In one source (NRAO 530, Fig. 1r), the spectral turnover is particularly prominent and well sampled by our observations. Cores in three sources, 0716+714 (Fig. 2a), OJ 287 (Fig. 2b), and 3C 454.3 (Fig. 2d), show inverted spectra which are slightly curved. The core spectrum of only one source (1510−089, Fig. 2c) can be adequately described by a simple power law in the whole 4.6–43.2 GHz frequency range. In the following, we focus on sources that show a well defined spectral turnover, and thus can be used to determine the physical conditions in the emitting plasma.

We fit a homogeneous synchrotron source model [10] (see the Appendix for more details) to the observed spectra in order to obtain the magnetic field strength and particle energy distribution. The sources for which the data reduction is complete are presented in Table I. For 13 sources, the model provided an adequate fit to the observed spectra (Fig. 1) while four sources exhibit flat or inverted spectra (Fig. 2) that cannot be described by the homogeneous synchrotron model.

4. Discussion

4.1. Model reliability

The physical parameters presented in Table I correspond to typical values for emitting electrons inside a large area of a few milliarcseconds in size (shaded areas on Fig. 1). In most cases, only an upper limit on the magnetic field strength could be placed, because most regions where the spectral turnover is detected remain unresolved. The results are consistent with estimates obtained by a method based on model-fitting bright VLBI components with 2D Gaussian components (see Fig. 3 for results on BL Lacertae). The model-fitting based method is described in detail in [3] where it was applied to 3C 273 and the average magnetic field strength $B_\perp \sim 10^{-2}$ G was obtained for the 8 GHz core region which is comparable in size to the region probed in our research. This value is in a good agreement with our upper limit at $B_\perp \leq 0.016$ G given in Table I.

4.2. Electron energy spectrum

The spectra above the synchrotron turnover are nearly flat or slightly inverted in core regions of all sources investigated in this work. This may result from blending of a few emitting regions with different peak frequencies (an example of such blending may be found in the core region of BL Lacertae, see the top right panel in Fig. 3, see also [3] for 3C 273). Alternatively, a nearly flat spectrum may imply a hard energy spectrum of the emitting electrons (as may be the case for the component B1 in the jet of BL Lacertae whose spectrum is presented in the lower right panel of Fig. 3; see also Table II). The hard electron spectrum is difficult to explain by the conventional first-order Fermi acceleration mechanism. However, the hard spectrum can be produced by the second-order Fermi mechanism ("stochastic acceleration") [11].

5. Summary and prospects

We have placed upper limits of $B_\perp \leq 10^{-2}$–10^{2} G (observer's frame) on the magnetic field strength in 13 out of 17 *Fermi* blazars (Table I). Spectra of four blazars could not be described by the simple homogeneous synchrotron source model, and no constraints on the magnetic field and particle energy spectrum could be obtained for these sources. Hard spectra ($-0.5 \leq \alpha \leq +0.1$, $S_\nu \sim \nu^\alpha$) observed in the blazar cores above the synchrotron peak may either indicate a hard energy spectrum of the relativistic electron population in the jet or result from significant inhomogeneity (of the magnetic field and plasma parameters or just optical depth) across the emitting region.

Since γ-ray emission in blazars is suggested to originate from regions spatially close to the VLBI core [12], the estimates of the magnetic field strength and electron energy distribution presented in Table I could be used to constrain broad-band Spectral Energy Distribution (SED) models. Simultaneously with the VLBA observations described here, *Swift* X-ray/ultraviolet/optical target of opportunity observations were performed. When combined with the *Fermi* γ-ray data this will provide a unique data set for the SED modeling. Analysis of this data set is presently underway.

Table I: Physical parameters estimation

IAU Name (B1950.0)	Alternative Name	Epoch	$p^{a,b}$	$B_{\perp}^{b,c}$ [G]	Comments
0235+164	AO 0235+16	2008-09-02	0.8	≤ 0.89	
0528+134		2008-10-02	1.4	≤ 0.12	
0716+714		2009-02-05			inverted spectrum $\alpha = 0.4$, model N/A[d]
0827+243	OJ 248	2009-04-09	1.6	≤ 3.4	
0851+202	OJ 287	2009-02-02			inverted spectrum $\alpha = 0.7$, model N/A[d]
1219+285	W Com	2009-05-14	0.8	≤ 108	preliminary analysis
1226+023	3C 273	2009-02-05	2.0	≤ 0.016	
1253−055	3C 279	2009-02-02	1.4	≤ 0.89	
1510−089		2009-04-09			inverted spectrum $\alpha = 0.2$, model N/A[d]
1633+383	4C 38.41	2009-06-20	1.0	≤ 0.24	preliminary analysis
1652+398	Mrk 501	2009-05-14	1.6	≤ 3.5	preliminary analysis
1730−130	NRAO 530	2009-06-20	1.6	≤ 3.6	preliminary analysis
1959+650		2008-10-23	1.4	≤ 17	
2155−304		2008-09-05	1.0	≤ 26	
2200+420	BL Lac	2008-09-02	1.0	≤ 0.44	
2251+158	3C 454.3	2008-10-02			inverted spectrum $\alpha = 0.8$, model N/A[d]
2344+514		2008-10-23	1.2	≤ 57	43 GHz data not included in the fit

[a] p is the power law index in the electron energy distribution $N(E) = N_0 E^{-p}$.
Note, that for the optically thin part of the synchrotron spectrum $p = 1 - 2\alpha$,
where α is defined as $S_\nu \sim \nu^\alpha$.

[b] The estimates correspond to the region of parsec-scale radio core.

[c] The values are in the observer's frame.

[d] The homogeneous synchrotron source model is not applicable for this spectrum.

Acknowledgments

K. Sokolovsky is supported by the International Max-Planck Research School (IMPRS) for Astronomy and Astrophysics at the universities of Bonn and Cologne. T. Savolainen is a research fellow of the Alexander von Humboldt foundation. T. Savolainen also acknowledges support by the Academy of Finland grant 120516. Y. Kovalev was supported by the return fellowship of Alexander von Humboldt foundation and the Russian Foundation for Basic Research (RFBR) grant 08-02-00545. This research has been partially funded by the Bundesministerium für Wirtschaft und Technologie under Deutsches Zentrum für Luft- und Raumfahrt grant number 50OR0808. This work is based on data obtained from the National Radio Astronomy Observatory's Very Long Baseline Array (VLBA), project BK150. The National Radio Astronomy Observatory is a facility of the National Science Foundation operated under cooperative agreement by Associated Universities, Inc. This research has made use of NASA's Astrophysics Data System; the NASA/IPAC Extragalactic Database (NED) which is operated by the JPL, Caltech, under contract with the NASA, the SIMBAD database, operated at CDS, Strasbourg, France. The authors are grateful to E. Ros for reviewing this manuscript.

References

1 Atwood W. B., et al., 2009, ApJ, 697, 1071
2 Zensus J. A., 1997, ARA&A, 35, 607
3 Savolainen T., Wiik K., Valtaoja E., Tornikoski M. 2008, ASPC, 386, 451
4 Lobanov, A. P. 1998, A&AS,132, 261
5 Napier P. J., 1994, IAUS, 158, 117
6 Fomalont E., 1981, NRAON, 3, 3
7 Shepherd M.C., Pearson T.J. and Taylor G.B. 1994, BAAS, 26, 987
8 Kovalev, Y. Y., Lobanov, A. P., Pushkarev, A. B., & Zensus, J. A. 2008, A&A, 483, 759
9 Lobanov, A. P. 1998, A&A, 330, 79
10 Pacholczyk A.G. 1970, Radio astrophysics, San Francisco: Freeman
11 Virtanen, J. J. P., & Vainio, R. 2005, ApJ, 621, 313
12 Kovalev, Y. Y., et al. 2009, ApJL, 696, L17
13 Marscher A.P. 1983, ApJ, 264, 296

Appendix: synchrotron source model used in pixel-based approach

Following [10], we consider a uniform cloud of relativistic electrons in the external uniform magnetic field with component $B_\perp$ perpendicular to the line of sight. We assume that the electron energy distribution is described by a power law:

$$N(E) = N_0 E^{-p},$$

where N_0 and p are constants. For this case, we can write the radiation transfer equation

$$\frac{dI_\nu}{ds} = -\kappa_\nu I_\nu + j_\nu,$$

where I_ν is the specific intensity at the frequency ν, ds is the differential element of path length, j_ν is the emission coefficient (emissivity), κ_ν is the absorption (extinction) coefficient. If j_ν and κ_ν are constant along the line of sight, the solution of the radiation transfer equation is

$$I_\nu = \int_0^L j_\nu e^{-\int_0^s \kappa_\nu ds} ds = \frac{j_\nu}{\kappa_\nu}(1 - e^{-\kappa_\nu L}),$$

where L is the size of the electron cloud along the line of sight, and $\kappa_\nu L = \tau_\nu$ is the optical depth.

Following [10], this solution can be written in the form:

$$I_\nu = S(\nu_1) J(\frac{\nu}{\nu_1}, p), \qquad (1)$$

where

$$\nu_1 = 2c_1 (N_0 L c_6(p))^{2/(p+4)} B_\perp^{(p+2)/(p+4)}, \qquad (2)$$

$$S(\nu_1) = \frac{c_5(p)}{c_6(p)} B_\perp^{-1/2} \frac{\nu_1}{2c_1}^{5/2}, \qquad (3)$$

$$J(z,p) = z^{5/2}(1 - \exp[-z^{-(p+4)/2}]),$$

$$c_1 = \frac{3e}{4\pi m_e^3 c^5} = 6.27 \times 10^{18},$$

$$c_3 = \frac{\sqrt{3}}{4\pi} \frac{e^3}{m_e c^2} = 1.87 \times 10^{-23},$$

$$c_5(p) = \frac{1}{4} c_3 \Gamma\left(\frac{3p-1}{12}\right) \Gamma\left(\frac{3p+7}{12}\right) \left(\frac{p+7/3}{p+1}\right),$$

$$c_6(p) = \frac{1}{32} \left(\frac{c}{c_1}\right)^2 c_3 \left(p + \frac{10}{3}\right) \Gamma\left(\frac{3p+2}{12}\right) \Gamma\left(\frac{3p+10}{12}\right),$$

where e is the electron charge, m_e is the electron mass, and c is the speed of light in vacuum.

The power law index p of the electron energy distribution may be found from the spectral index α ($S_\nu \sim \nu^\alpha$) in the optically thin part of the spectrum: $p = 1 - 2\alpha$. The optical depth τ_m corresponding to the observed spectral peak frequency ν_m may be found from equation $\exp[\tau_m] = 1 + \frac{p+4}{5}\tau_m$.

The frequency ν_1 corresponding to $\tau_{\nu_1} = 1$ may be found from ν_m, p and τ_m: $\nu_1 = \tau_m^{2/(p+4)} \nu_m$.

From equations (1), (2) and (3), we can derive the perpendicular component of the magnetic field:

$$B_\perp = \left(\frac{c_5(p)}{c_6(p)}\right)^2 S(\nu_1)^{-2} \left(\frac{\nu_1}{2c_1}\right)^5. \qquad (4)$$

Note, that if the size of an emitting region is smaller then the angular resolution, only a *lower limit* on the intensity and, correspondingly, an *upper limit* on the magnetic field $B_\perp$ can be derived.

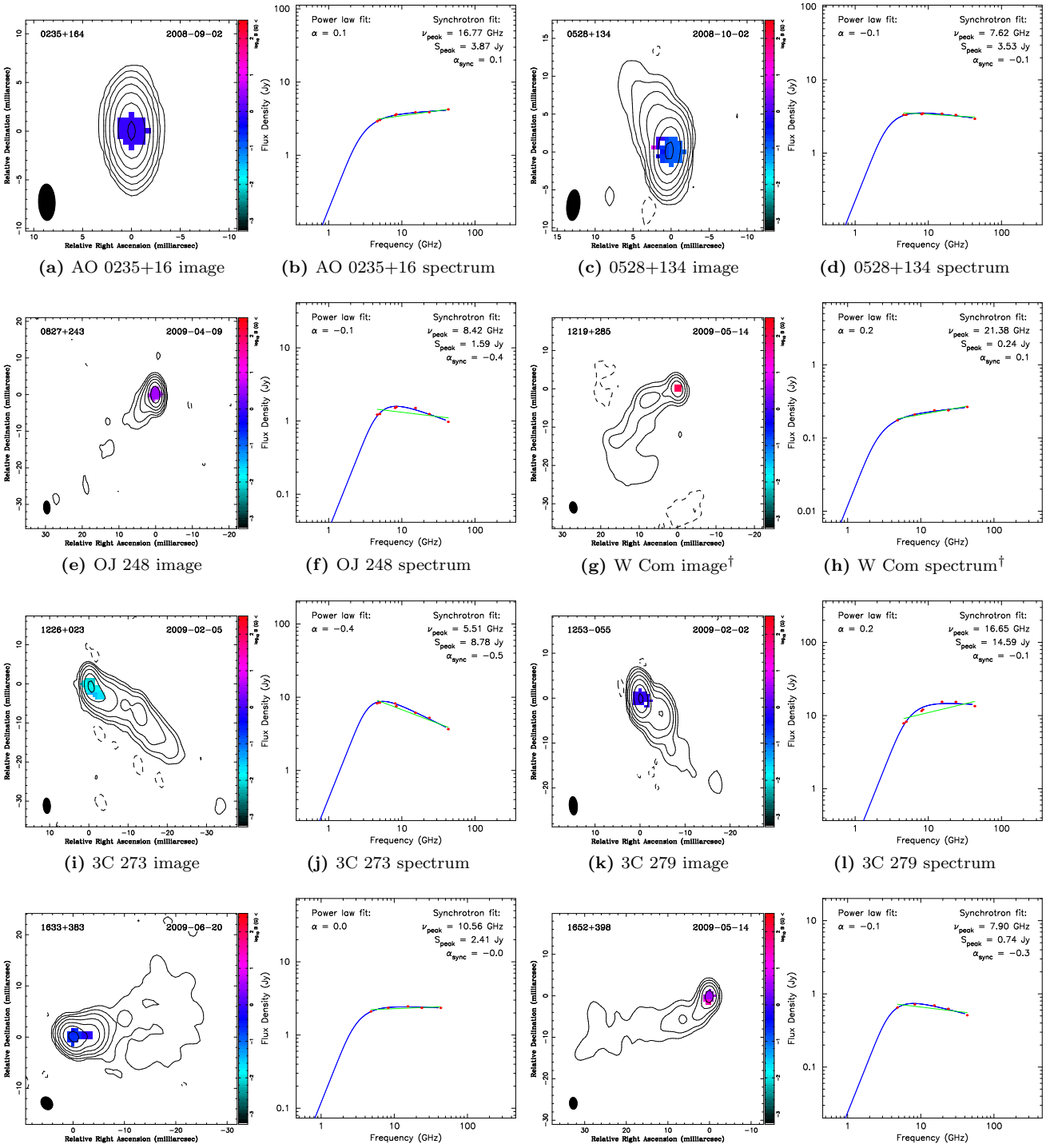

(a) AO 0235+16 image **(b)** AO 0235+16 spectrum **(c)** 0528+134 image **(d)** 0528+134 spectrum

(e) OJ 248 image **(f)** OJ 248 spectrum **(g)** W Com image† **(h)** W Com spectrum†

(i) 3C 273 image **(j)** 3C 273 spectrum **(k)** 3C 279 image **(l)** 3C 279 spectrum

(m) 4C 38.41 image† **(n)** 4C 38.41 spectrum† **(o)** Mrk 501 image† **(p)** Mrk 501 spectrum†

Figure 1: VLBI images at 8.4 GHz and radio continuum spectra of sources for which the synchrotron self-absorption turnover frequency was successfully measured. The shaded area on the images marks the region where the synchrotron turnover was detected. The color of the shaded area represents the upper limit of the magnetic field strength ($B_\perp$). The values of $B_\perp$ and p presented in Table I correspond to this area. On the spectrum plots, the blue curves represent the homogeneous synchrotron source model, while the green lines represent a simple power law model. Best fit parameters of both models are shown on each plot. The † symbol marks sources for which the analysis results are preliminary.

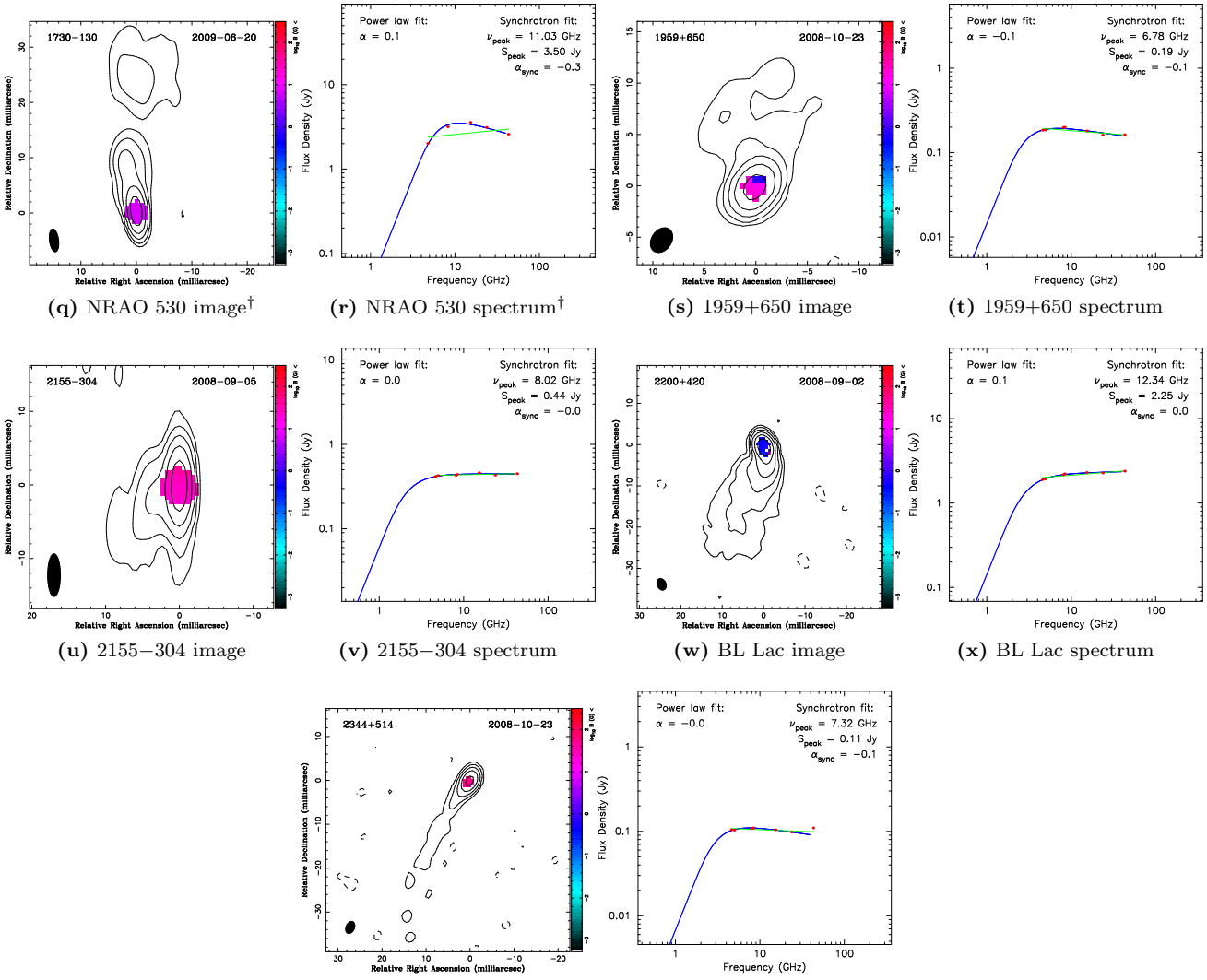

(q) NRAO 530 image† **(r)** NRAO 530 spectrum† **(s)** 1959+650 image **(t)** 1959+650 spectrum

(u) 2155−304 image **(v)** 2155−304 spectrum **(w)** BL Lac image **(x)** BL Lac spectrum

(y) 2344+514 image **(z)** 2344+514 spectrum

Figure 1: continued

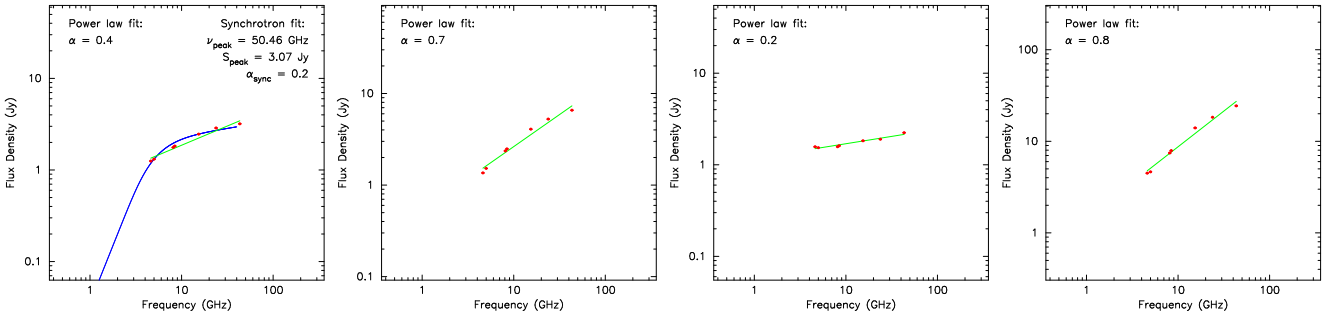

(a) 0716+714 spectrum **(b)** OJ 287 spectrum **(c)** 1510−089 spectrum **(d)** 3C 454.3 spectrum

Figure 2: VLBA spectra of sources whose spectra cannot be adequately described by the simple homogeneous model. The spectra correspond to parsec-scale core regions. Green lines represent a power law fit. It is possible to fit a homogeneous synchrotron source model (blue curve) to the observed spectrum of 0716+714, however, a simple power law provides better (lower χ^2) fit.

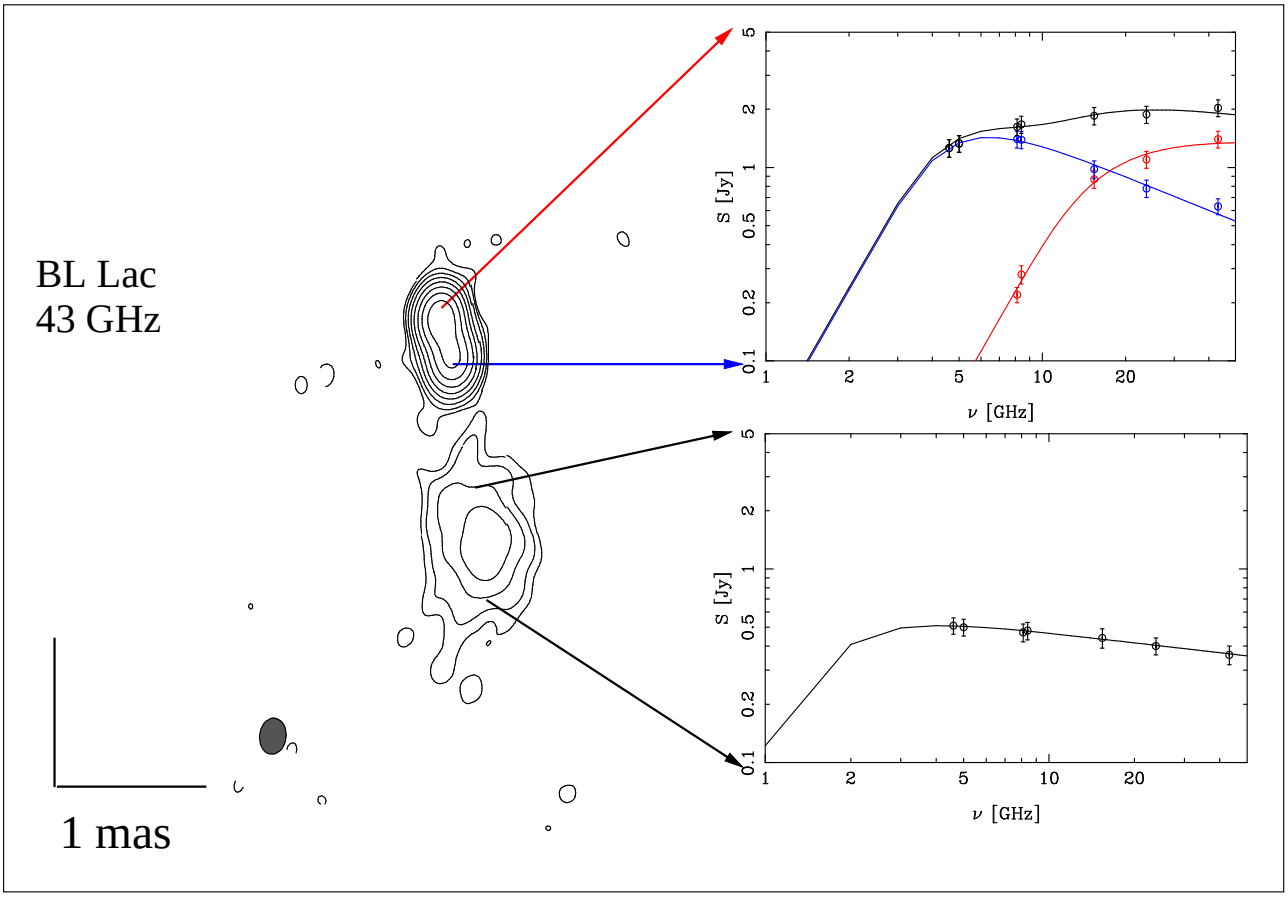

Figure 3: Results of the model-fitting based analysis of BL Lacertae (2200+420). The contours represent the CLEAN image at 43 GHz, the beam size and the linear scale are indicated at the lower left panel. The source structure was approximated with Gaussian components (see Table II). The fitting was conducted in the the *uv*-plane. The two inner components (C1 its position is marked by the red arrow, C2 marked by the blue arrow) are unresolved while the third component (B1 marked by two black arrows) is resolved at 43 GHz. Fig. 1x presents the spectrum of this source obtained in the course of pixel-based analysis. This spectrum corresponds to the combined spectrum (black) of components C1 (red) and C2 (blue) presented in the upper right panel of the current figure. The peak frequency for B1 is not well constrained, however, following [13] we can put an upper limit on the magnetic field strength in this component $B < 0.06$ G (observer's frame).

Table II: BL Lacertae model component parameters

Component	Distance [mas]	ν_m [GHz]	S_m [Jy]	α
C1 (core)	0	> 43	> 1.02	...
C2	0.26	6.4	1.43	-0.58
B1	1.47	< 4.1	> 0.51	-0.17

ν_m — synchrotron self-absorption peak frequency.
S_m — synchrotron self-absorption peak flux density.
α — spectral index in the optically thin part of the spectrum.